iScience, Volume *26*

Supplemental information

Modulation of microglial metabolism facilitates regeneration in demyelination

Chuan Qin, Sheng Yang, Man Chen, Ming-Hao Dong, Luo-Qi Zhou, Yun-Hui Chu, Zhu-Xia Shen, Dale B. Bosco, Long-Jun Wu, Dai-Shi Tian, and Wei Wang

Supplementary Figure 1-6 and Figure legends

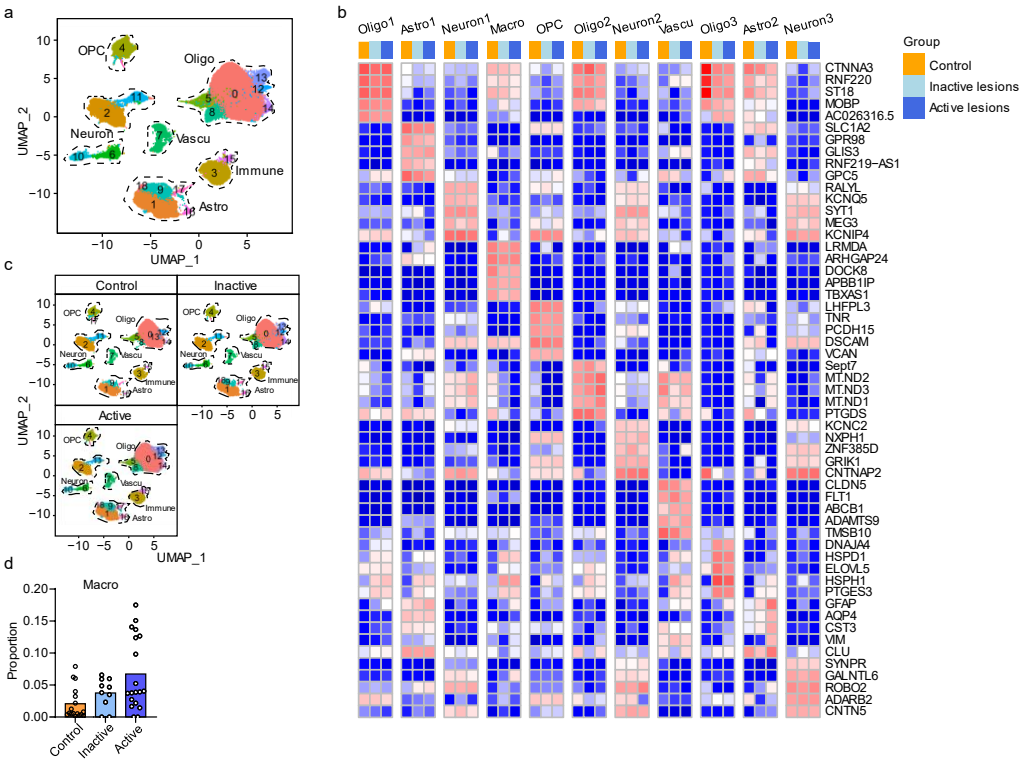

Supplementary Fig.1 Single-nuclei RNA sequencing identifies changes in major brain cell types in healthy control, MS inactive lesions and MS active lesions, related to Fig 1.

a. Single-nuclei RNA sequencing (snRNA-seq) initial mapping (UMAP plot) and annotations based on the top differentially expressed genes in each cluster after re-analysis of raw data from Schirmer et al, [15] Jäkel et al, [16] and Absinta et al. [17]

b. Heatmap showing distinct cell types identified by cell-type-specific markers.

c. Overview of all cell populations in healthy control, MS inactive lesions and MS active lesions by UMAP plots.

d. Relative frequency of "microglia/macrophages" cluster in each group. The Y axis range is 0 to 1.

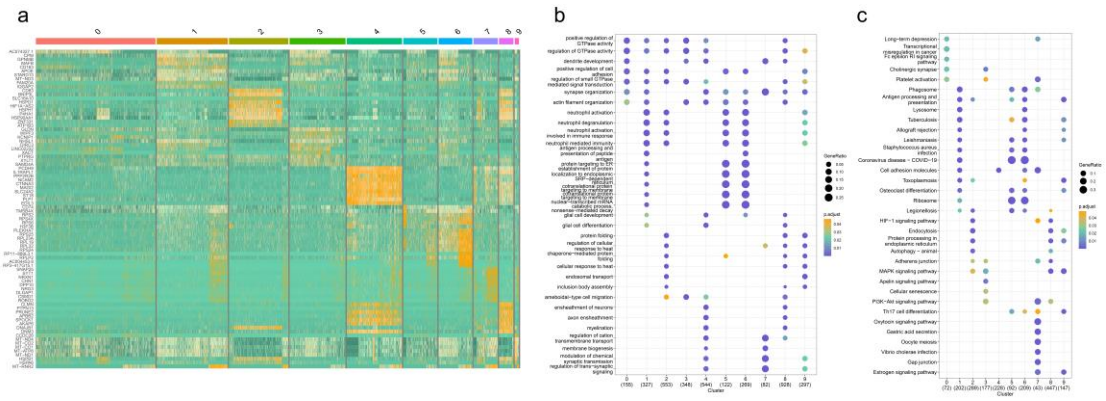

Supplementary Fig. 2 Transcriptional profiles and functional enrichment of different microglial subclusters, related to Fig 1.

a. Heatmap illustrating transcriptional profiles of different microglial subclusters

b. Biological processes (BP) enrichment of different microglial subclusters.

c. KEGG signaling pathways enrichment of different microglial subclusters.

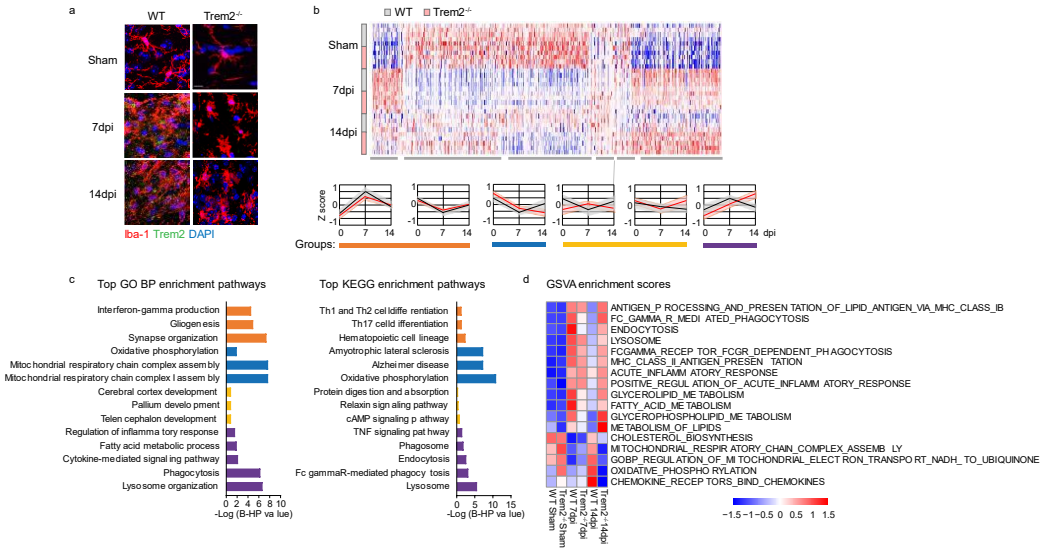

Supplementary Fig. 3 Trem2 deficiency induces pronounced and sustained alterations in microglial transcriptome during acute demyelination and remyelination in vivo, related to Fig 5.

a, Representative images of Iba-1 (red), Trem2 (green) and DAPI (blue) immunostaining in Trem2$^{-/-}$ mice and wild-type control with LPC injection. Scale bar, 20μm.

b-c, Transcriptome analysis was performed using RNA sequencing of microglia sorted from the following groups of mice: sham Trem2$^{-/-}$ and control mice, Trem2$^{-/-}$ and control mice at 7 dpi, and Trem2$^{-/-}$ and control mice at 14 dpi. n = 4-5 mice per group. Heatmap depicting gene clusters associated with genotype and disease stage based on transcripts that displayed a P value <0.01 and fold change >1.5. The scale represents Z-score–transformed expression values (with red and blue indicating up-regulated and down-regulated genes, respectively, compared with the mean value of a gene from all samples). These gene clusters were further grouped according to their pattern of expression into the four groups that were analyzed using GO and KEGG to annotate significance.

d, Heatmap showing the differences in biological processes by GSVA enrichment scores among the different groups.

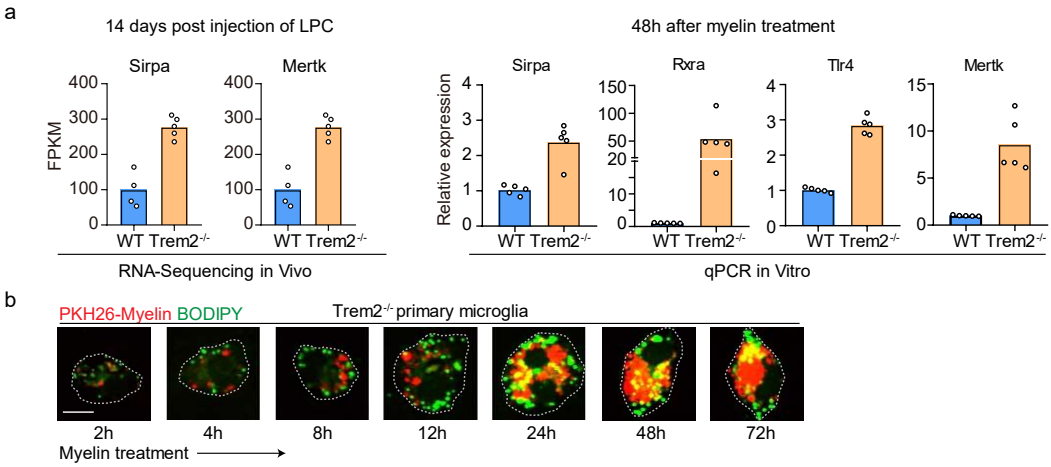

Supplementary Fig. 4 Compensatory phagocytosis and impaired lipid metabolism in Trem2$^{-/-}$ microglia, related to Fig 5, 6 and 7.

a, Quantification of transcriptional expression via RNA sequencing of sorted microglia from control and Trem2$^{-/-}$ mice at 14 dpi, and RT-PCR analysis of gene expression in Trem2$^{-/-}$ and wild-type microglia 48h after myelin debris treatment. n = 4-5 mice per group, or 5 biologically independent replicates.

b, Representative images of PKH26-Myelin (red), and BODIPY (green) immunostaining in Trem2$^{-/-}$ with myelin treatment. Scale bar, 10μm.

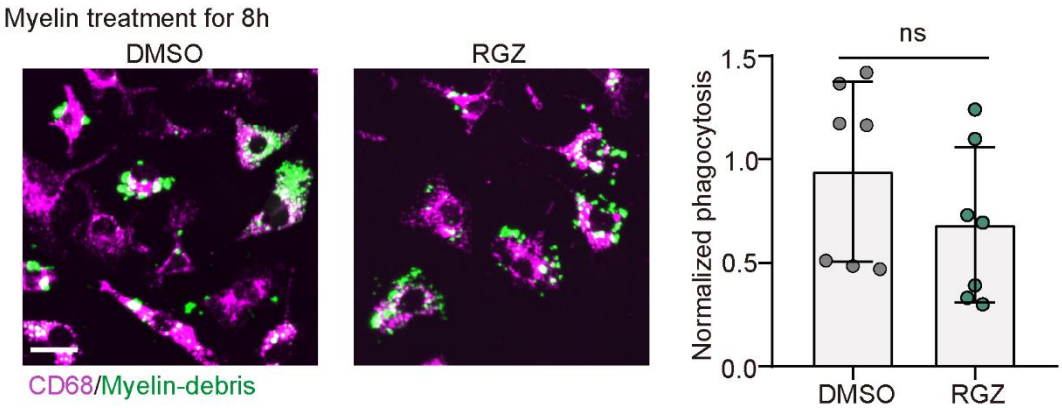

Supplementary Fig. 5 Phagocytosis in myelin debris treated microglia with or without rosiglitazone, related to Fig 6.

Representative images and quantification of phagocytosis in myelin debris treated microglia with or without rosiglitazone. Scale bar, 20μm. Normalized intensity of myelin debris shown as n = 7 biologically independent replicates, mean ± SD, unpaired t-test.

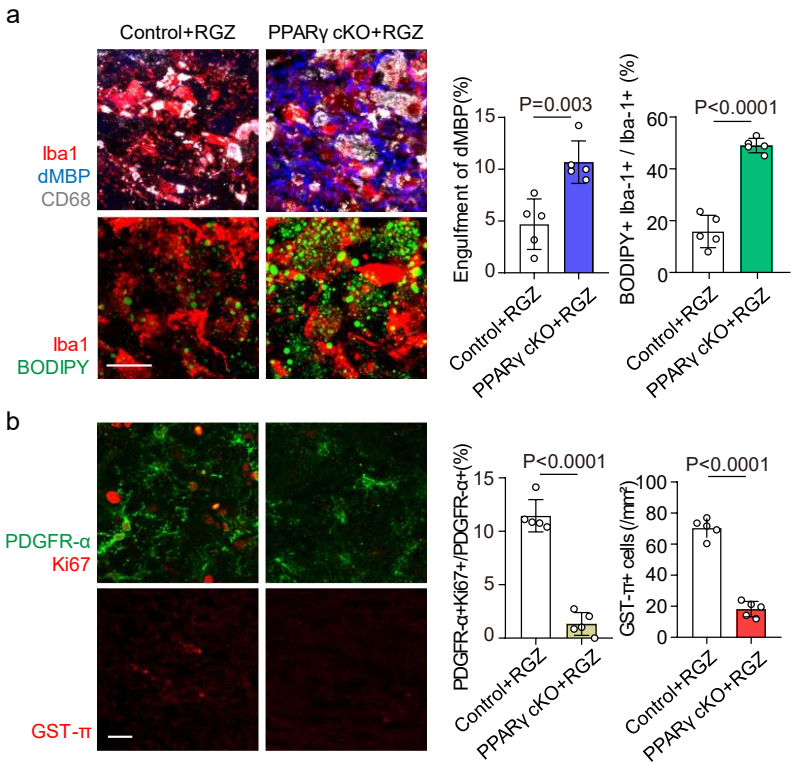

Supplementary Fig. 6 Rosiglitazone administration promoted microglial remyelination via PPAR-γ signaling pathway, related to Fig 7.

a, Representative images of Iba-1 (red), dMBP (blue) and CD68 (white), or Iba-1 (red) and BODIPY (green) immunostaining in microglia-specific PPAR-γ deficient mice (Cx3cr1CreER$^{+/-}$PPAR-γ$^{fl/fl}$, PPAR-γ cKO) or littermate controls with rosiglitazone treatment at 7 dpi. Scale bar, 20 μm. Quantification of dMBP within microglia and the percentage of BODIPY^{+} Iba-1^{+} in Iba-1^{+} cells. n = 5 mice per group, mean ± SD, unpaired t test.

b, Representative images of PDGFR-α (green) and Ki67 (red), and GST-π (red) immunostaining in PPAR-γ cKO mice or littermate controls with rosiglitazone treatment at 7 dpi. Scale bar, 20 μm. Quantification of the percentage of proliferating OPCs (PDGFR-α^{+}Ki67^{+}/PDGFR-α^{+} cells), and mature oligodendrocytes (GST-π^{+}) densities. n = 5 mice per group, mean ± SD, unpaired t test.

Reference

1. Sariol, A., Mackin, S., Allred, M.G., Ma, C., Zhou, Y., Zhang, Q., Zou, X., Abrahante, J.E., Meyerholz, D.K., and Perlman, S. (2020). Microglia depletion exacerbates demyelination and impairs remyelination in a neurotropic coronavirus infection. Proc Natl Acad Sci U S A *117*, 24464-24474.http://doi.org/10.1073/pnas.2007814117.
2. Chen, M., Yang, L.L., Hu, Z.W., Qin, C., Zhou, L.Q., Duan, Y.L., Bosco, D.B., Wu, L.J., Zhan, K.B., Xu, S.B., and Tian, D.S. (2020). Deficiency of microglial Hv1 channel is associated with activation of autophagic pathway and ROS production in LPC-induced demyelination mouse model. J Neuroinflammation *17*, 333.http://doi.org/10.1186/s12974-020-02020-y.
3. Qin, C., Liu, Q., Hu, Z.W., Zhou, L.Q., Shang, K., Bosco, D.B., Wu, L.J., Tian, D.S., and Wang, W. (2018). Microglial TLR4-dependent autophagy induces ischemic white matter damage via STAT1/6 pathway. Theranostics *8*, 5434-5451.http://doi.org/10.7150/thno.27882.
4. Schafer, D.P., Lehrman, E.K., Kautzman, A.G., Koyama, R., Mardinly, A.R., Yamasaki, R., Ransohoff, R.M., Greenberg, M.E., Barres, B.A., and Stevens, B. (2012). Microglia sculpt postnatal neural circuits in an activity and complement-dependent manner. Neuron *74*, 691-705.http://doi.org/10.1016/j.neuron.2012.03.026.
5. Werneburg, S., Jung, J., Kunjamma, R.B., Ha, S.K., Luciano, N.J., Willis, C.M., Gao, G., Biscola, N.P., Havton, L.A., Crocker, S.J., et al. (2020). Targeted Complement Inhibition at Synapses Prevents Microglial Synaptic Engulfment and Synapse Loss in Demyelinating Disease. Immunity *52*, 167-182 e167.http://doi.org/10.1016/j.immuni.2019.12.004.
6. Liu, L., Besson-Girard, S., Ji, H., Gehring, K., Bulut, B., Kaya, T., Usifo, F., Simons, M., and Gokce, O. (2021). Dissociation of microdissected mouse brain tissue for artifact free single-cell RNA sequencing. STAR Protoc *2*, 100590.http://doi.org/10.1016/j.xpro.2021.100590.
7. Carlstrom, K.E., Zhu, K., Ewing, E., Krabbendam, I.E., Harris, R.A., Falcao, A.M., Jagodic, M., Castelo-Branco, G., and Piehl, F. (2020). Gsta4 controls apoptosis of differentiating adult oligodendrocytes during homeostasis and remyelination via the mitochondria-associated Fas-Casp8-Bid-axis. Nat Commun *11*, 4071.http://doi.org/10.1038/s41467-020-17871-5.
8. Liu, K.M., and Shen, C.L. (1985). Ultrastructural sequence of myelin breakdown during Wallerian degeneration in the rat optic nerve. Cell Tissue Res *242*, 245-256.http://doi.org/10.1007/BF00214537.
9. Savage, J.C., Picard, K., Gonzalez-Ibanez, F., and Tremblay, M.E. (2018). A Brief History of Microglial Ultrastructure: Distinctive Features, Phenotypes, and Functions Discovered Over the Past 60 Years by Electron Microscopy. Front Immunol *9*, 803.http://doi.org/10.3389/fimmu.2018.00803.
10. Marschallinger, J., Iram, T., Zardeneta, M., Lee, S.E., Lehallier, B., Haney, M.S., Pluvinage, J.V., Mathur, V., Hahn, O., Morgens, D.W., et al. (2020). Lipid-droplet-accumulating microglia represent a dysfunctional and proinflammatory state in the aging brain. Nat Neurosci *23*, 194-208.http://doi.org/10.1038/s41593-019-0566-1.
11. Nugent, A.A., Lin, K., van Lengerich, B., Lianoglou, S., Przybyla, L., Davis, S.S., Llapashtica, C., Wang, J., Kim, D.J., Xia, D., et al. (2020). TREM2 Regulates Microglial Cholesterol Metabolism upon Chronic Phagocytic Challenge. Neuron *105*, 837-854

e839.http://doi.org/10.1016/j.neuron.2019.12.007.

12. Cantuti-Castelvetri, L., Fitzner, D., Bosch-Queralt, M., Weil, M.T., Su, M., Sen, P., Ruhwedel, T., Mitkovski, M., Trendelenburg, G., Lutjohann, D., et al. (2018). Defective cholesterol clearance limits remyelination in the aged central nervous system. Science *359*, 684-688.http://doi.org/10.1126/science.aan4183.

13. Hu, Y., Mai, W., Chen, L., Cao, K., Zhang, B., Zhang, Z., Liu, Y., Lou, H., Duan, S., and Gao, Z. (2020). mTOR-mediated metabolic reprogramming shapes distinct microglia functions in response to lipopolysaccharide and ATP. Glia *68*, 1031-1045.http://doi.org/10.1002/glia.23760.

14. Zhou, T., Zheng, Y., Sun, L., Badea, S.R., Jin, Y., Liu, Y., Rolfe, A.J., Sun, H., Wang, X., Cheng, Z., et al. (2019). Microvascular endothelial cells engulf myelin debris and promote macrophage recruitment and fibrosis after neural injury. Nat Neurosci *22*, 421-435.http://doi.org/10.1038/s41593-018-0324-9.

15. Schirmer, L., Velmeshev, D., Holmqvist, S., Kaufmann, M., Werneburg, S., Jung, D., Vistnes, S., Stockley, J.H., Young, A., Steindel, M., et al. (2019). Neuronal vulnerability and multilineage diversity in multiple sclerosis. Nature *573*, 75-82.http://doi.org/10.1038/s41586-019-1404-z.

16. Jakel, S., Agirre, E., Mendanha Falcao, A., van Bruggen, D., Lee, K.W., Knuesel, I., Malhotra, D., Ffrench-Constant, C., Williams, A., and Castelo-Branco, G. (2019). Altered human oligodendrocyte heterogeneity in multiple sclerosis. Nature *566*, 543-547.http://doi.org/10.1038/s41586-019-0903-2.

17. Absinta, M., Maric, D., Gharagozloo, M., Garton, T., Smith, M.D., Jin, J., Fitzgerald, K.C., Song, A., Liu, P., Lin, J.P., et al. (2021). A lymphocyte-microglia-astrocyte axis in chronic active multiple sclerosis. Nature *597*, 709-714.http://doi.org/10.1038/s41586-021-03892-7.